Granular Matter (2020) 22:85
https://doi.org/10.1007/s10035-020-01052-8

ORIGINAL PAPER

DEM simulation of anisotropic granular materials: elastic and inelastic behavior

Giuseppina Recchia[1] · Vanessa Magnanimo[2] · Hongyang Cheng[2] · Luigi La Ragione[1]

Received: 31 July 2019
© The Author(s) 2020

Abstract
In this work, Discrete Elements Method simulations are carried out to investigate the effective stiffness of an assembly of frictional, elastic spheres under anisotropic loading. Strain probes, following both forward and backward paths, are performed at several anisotropic levels and the corresponding stress is measured. For very small strain perturbations, we retrieve the linear elastic regime where the same response is measured when incremental loading and unloading are applied. Differently, for a greater magnitude of the incremental strain a different stress is measured, depending on the direction of the perturbation. In the case of unloading probes, the behavior stays elastic until non-linearity is reached.Under forward perturbations, the aggregate shows an intermediate *inelastic* stiffness, in which the main contribution comes from the normal contact forces. That is, when forward incremental probes are applied the behavior of anisotropic aggregates is an incremental frictionless behavior. In this regime we show that contacts roll or slide so the incremental tangential contact forces are zero.

Keywords Granular materials · Micromechanics · Discrete Element Method · Effective moduli

1 Introduction

Granular media are complex systems widely present in civil engineering in the form of soils or granulates, in industry including chemical synthesis, food production, thermal insulation, additive manufacturing and other application consisting of granular beds. Understanding the mechanical response of granular materials is important to elucidate fundamental aspects of the behavior of these particulate systems [1, 2]. To this end, numerical simulations, laboratory experiments and theoretical models have been employed. In particular, an interesting activity regards the theoretical analysis, developed in order to establish predictive models that should reproduce what seen in numerical simulations and/or laboratory experiments. There are models based upon a phenomenological approach and other based on micro-mechanics. The latter are more favorable when compared with Discrete Element Method (DEM) simulations [3] because it is possible to test not only the macroscopic response of the aggregate but also local features that characterize particle interactions. In this paper, we focus on a numerical analysis for a granular aggregate, referring to theoretical models already available in literature. In fact, it is not our goal to develop a new theory but to provide new insights of the elasto-plastic regime. We are interested to the incremental response of dense, sheared granular samples and how the response qualitatively changes as anisotropy develops in the aggregate. This is an important point, for example in the context of seismic waves that propagate in granular materials (e.g. [4, 5]), geotechnical applications involving regions where deformations are small [6], the development of elastic-plastic constitutive models, where elasticity needs a proper description, e.g. [7, 8] or as indicator for localization [9]. Several approaches have been used to investigate elasticity numerically, e.g., dynamical unloading probes [10–12], response envelope [13–15], stiffness matrix [16, 17], wave propagation [4, 18, 19], depending on the specific focus and

✉ Giuseppina Recchia
giuseppina.recchia@poliba.it

Vanessa Magnanimo
v.magnanimo@utwente.nl

Hongyang Cheng
h.cheng@utwente.nl

Luigi La Ragione
luigi.laragione@poliba.it

1 Politecnico di Bari, Via Edoardo Orabona, 4, Bari 70126, BA, Italy

2 MSM, TFE, Mesa+, University of Twente, Enschede, P.O.Box 217, 7500, AE, Netherlands

Published online: 30 September 2020

final goal. In particular, procedures (and often conclusions) diverge if the interest is on "pure" elasticity at very small strains or an elasto-plastic framework.

Here we study elasticity in granular materials over a wide range of strain magnitudes, for different directions and degrees of anisotropy. We highlight that the mechanical response of anisotropic granular aggregates is different if forward or backward incremental strain are applied. Beside the well-known linear elastic regime in which the same stress is measured when both forward and backward incremental strains are applied, we recognize a second regime, associated with greater perturbations, that proceed the non-linear behavior, i.e. the stiffness depends on the strain amplitude. We identify in this regime an *inelastic* stiffness in which the response becomes incrementally frictionless and the major symmetry of the macroscopic stiffness is lost (e.g. [20, 21]). Key parameters are the magnitude and direction of the probes applied to stressed, anisotropic states, compared with the strain under which the aggregate is initially loaded. In such framework, Froiio and Roux [17], Calvetti et al. [15], Kuhn et al. [22] use response envelopes obtained via DEM multidirectional loading probes to investigate the validity of common assumptions of elasto-plastic models for granular materials subjected to anisotropic loading paths. We, instead, operate with limited loading conditions because we have a different goal. Specifically, we focus on probes parallel and orthogonal to the initial monotonic loading in order to unravel the role of contacts elasticity, sliding and rolling in the transition of the elastic, inelastic, and plastic regime where the loss of symmetry emerges.

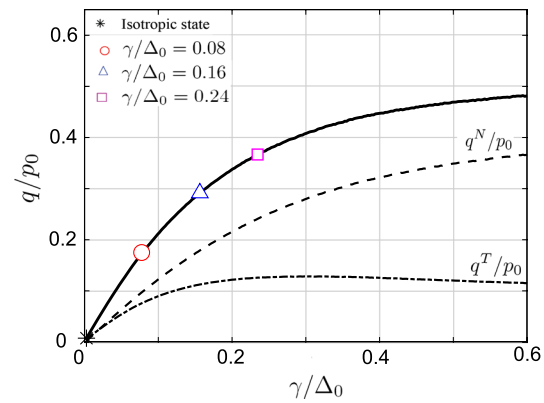

Fig. 1 Normalized deviatoric stress versus normalized deviatoric strain (solid line) and its components q_N/p_0 (dashed line) and q_T/p_0 (dotted line). Markers indicate the states where probes are applied

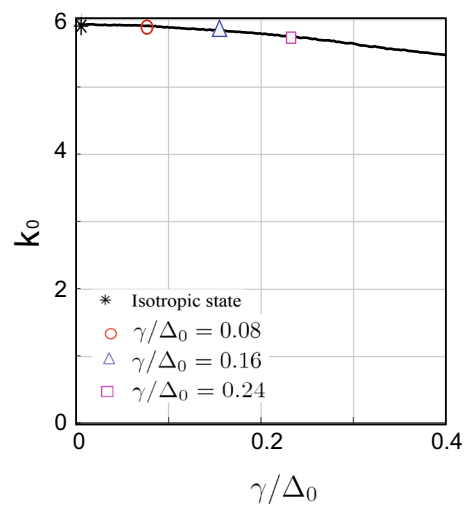

Fig. 2 Coordination number versus normalized deviatoric strain. Markers indicate the states where probes are applied

2 Numerical simulations

The DEM methods (e.g. [3, 23]) are a powerful tool to study granular materials in combination with theoretical models (e.g. [24–26]) to predict the material response under different loading conditions (e.g. [10–12, 27–29])

The code is based upon the knowledge of particles position and interaction forces. If the contact forces, acting on a particle, are known the problem is reduced to the integration of Newton's equations of motion for the translational and rotational degrees of freedom of that particle. The system considered here is a random assembly of identical, frictional, elastic spheres that interact through contacts in which gravity is neglected. A micro-mechanical analysis shows interesting features associated with the possibility that particles slide or roll.

2.1 Contact mechanics

For a given pair of particles, the interaction is represented by a non-central contact force

$$F_i = F^N \hat{d}_i + F^T \hat{t}_i, \tag{1}$$

where $\hat{d}_i$ is the unit contact vector that joins the centers of contacting particles and $\hat{t}_i$ is the tangential unit contact vector in the plane perpendicular to $\hat{d}_i$. The normal force F^N follows the non-linear Hertz law. F^T is the tangential contact force that incorporates a bilinear relationship, i.e., an elastic resistance followed by Coulomb sliding [30]. When $F^T \geq \mu F^N$, the tangential force in the slip direction is $F^T = \mu F^N$ [31].

The average stress σ_{ij} of the aggregate, according to Cauchy [32], is given by

$$\sigma_{ij} = \frac{1}{V} \sum_{c=1}^{N^c} F_i d_j \tag{2}$$

in which the sum is extended to all N^c contacts in the representative volume V. As in [33] and [28], the stress may be partitioned into its normal and tangential components

$$\sigma_{ij}^N = \frac{1}{V}\sum_{c=1}^{N^c} F^N \hat{d}_i^c d_j^c \tag{3}$$

and

$$\sigma_{ij}^T = \frac{1}{V}\sum_{c=1}^{N^c} F^T t_i^c d_j^c \tag{4}$$

in order to capture the relative contribution of the two parts.

2.2 Preparation protocol

We employ material properties typical of glass spheres, shear modulus $G = 29$GPa and Poisson's ratio, $\nu = 0.2$. We use an aggregate of $N = 10,000$ spheres, each with radius $R = 0.1$mm, randomly generated in a periodic cubic cell. Our calculations begin with a numerical protocol designed to mimic the experimental procedures used to prepare densely packed granular materials. Particles are then isotropically compressed without friction, $\mu = 0$, until a solid volume fraction slightly lower than random close-packing $\phi \leq \phi_{RCP}$ has been reached ($\phi_{RCP} \simeq 0.64$ for monodisperse aggregates [34]). Then, the particles are allowed to relax and reach pressure and coordination number equal to zero [11].

Furthermore, an isotropic compression is applied with friction coefficient $\mu = 0$ to reach the target value of mean stress $p_0 = 200$kPa, followed by a new relaxation stage under which the final friction coefficient is set to be $\mu = 0.5$. In this reference isotropic configuration, the solid volume fraction reaches $\phi = 0.64$ and the coordination number (the average number of contacts per particle) $k_0 = 5.95$, while the volumetric strain associated with the pressure p_0 is $\Delta_0 = 1 \times 10^{-3}$. This measure of the strain is based upon a theoretical prediction proposed by Jenkins et al. [35] in which, in a succession of isotropic states, pressure and volume strain are related by:

$$\Delta_0^{3/2} = \frac{\sqrt{3}\pi 9(1-\nu)}{k_0 \phi 2G} p_0. \tag{5}$$

whose incremental formulation is

$$\frac{3p_0}{2\Delta_0} = \frac{\delta p_0}{\delta \Delta_0}. \tag{6}$$

Given the pressure p_0 and the bulk modulus of the aggregate, i.e. $\delta p_0/\delta\Delta_0$, Eq. 6 permits to determine Δ_0.

2.3 Axial-symmetric compression

After the isotropic compression, an axial-symmetric deformation is applied along the direction $\mathbf{e}_1$. We take the friction coefficient $\mu = 0.5$, although glass beads are characterized by a smaller value, $\mu = 0.3$, because we obtain a smoother

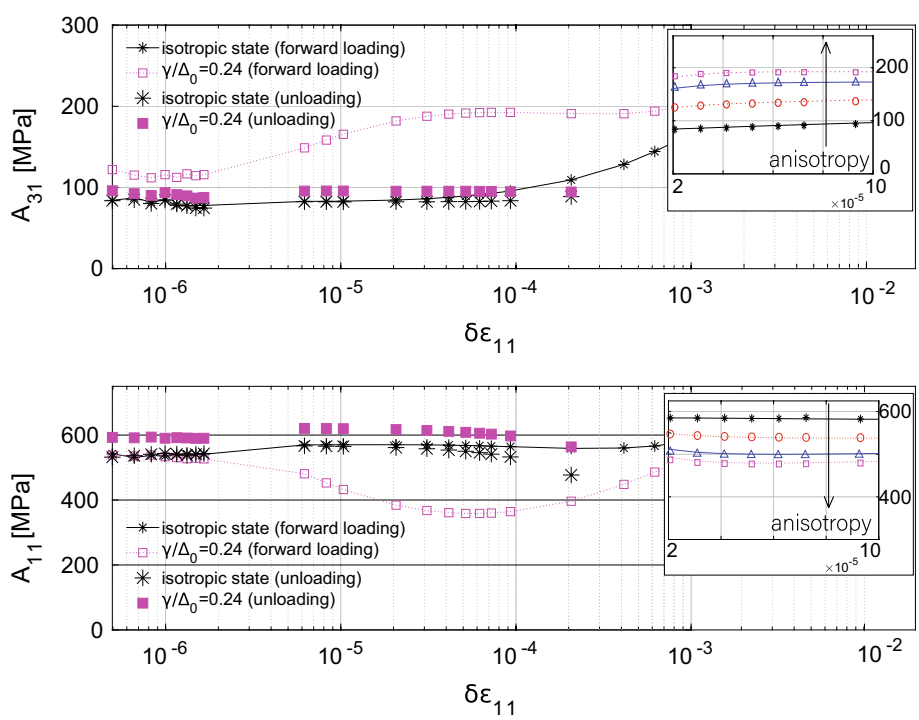

Fig. 3 Effective moduli A_{31} and A_{11} for different regimes of perturbation in two stressed states: isotropic and anisotropic state ($\gamma/\Delta_0 = 0.24$). In the insets the behaviour in the intermediate regime for all isotropic/anisotropic states, as indicated in Fig. 1 are shown

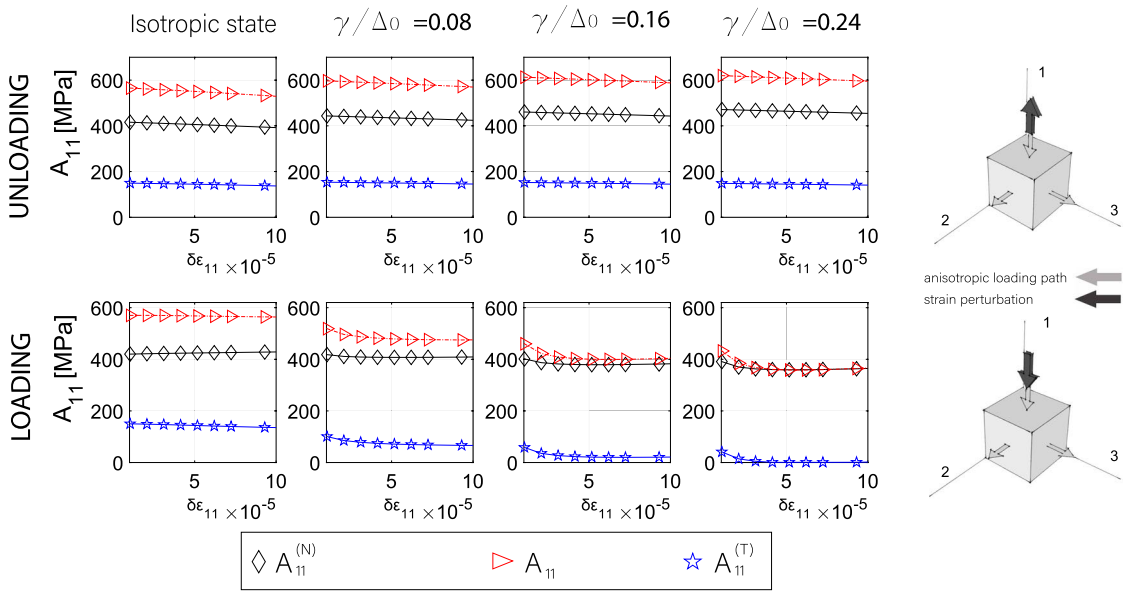

(a) A_{11} plotted in the second regime of perturbation: unloading and forward loading. In the forward loading, as anisotropy develops, the contribution of the tangential force in A_{11} becomes negligible.

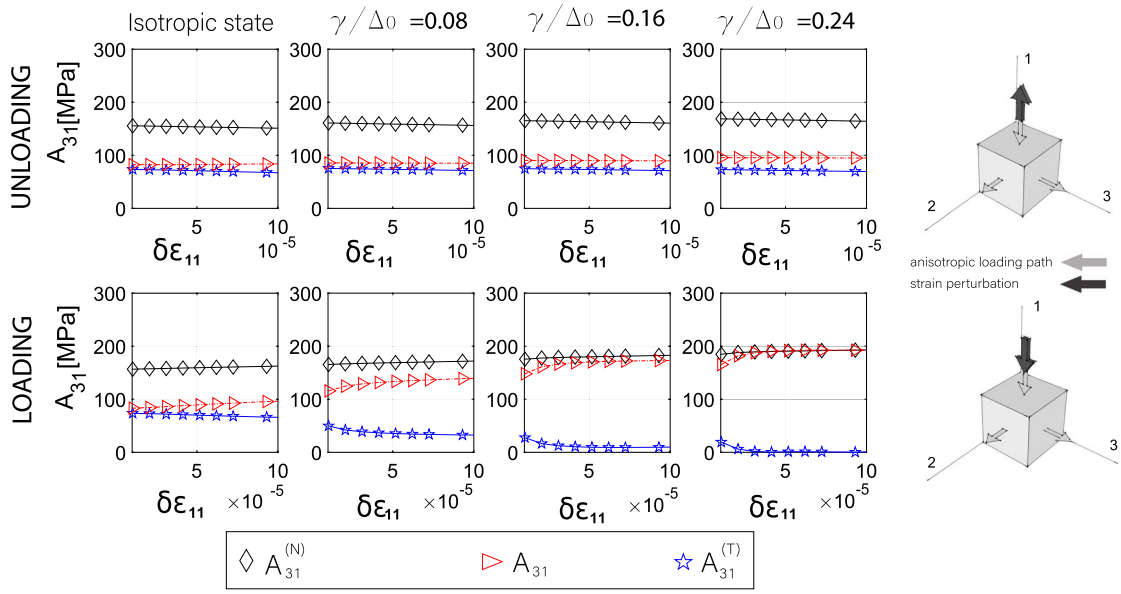

(b) A_{31} plotted in the second regime of perturbation: unloading and forward loading. In the forward loading, as anisotropy develops, the contribution of the tangential force in A_{31} becomes negligible.

Fig. 4 Effective moduli A_{11} and A_{31} versus strain amplitude

response with a an almost identical behavior. The test is carried out at constant mean stress, $p_0 = 200$ kPa, by means of a servo-mechanism [28]. To ensure quasi-static conditions, the compression is performed with a sequence of small strain steps, $\delta\varepsilon_{11} \simeq -10^{-5}$ (compression < 0 in our convention), and relaxation steps in which particles are allowed to dissipate kinetic energy and to reach intermediate equilibrium states. At each time step, along the compression path, we measure the deviatoric stress

$$q = \frac{1}{2}\left(\frac{\sigma_{22} + \sigma_{33}}{2} - \sigma_{11}\right) \tag{7}$$

and the normal and tangential parts q_N and q_T derived by means of Eqs. 3 and 4 , respectively [33]. In this work, we limit our analysis to a relative small range of deformation, $\gamma/\Delta_0 < 0.4$, in which $\gamma = (\epsilon_{22} + \epsilon_{33})/4 - \epsilon_{11}/2$ deviatoric strain applied. However, in this regime, contacts already experience elastic deformation, sliding and deletion [26]. In

Fig. 1 we plot the normalized deviatoric stress q/p_0 against the normalized deviatoric strain γ/Δ_0. In the same figure, the partition of the deviatoric stress into the normal and tangential contributions q_N/p_0 and q_T/p_0 is shown as well. After an initial similar response for q_N/p_0 and q_T/p_0, it is clear that the deviatoric stress is almost identifiable with its normal component, q_N/p_0. In this rather narrow regime of deformation the change in the coordination number (see Fig. 2), is negligible as well as in the fabric and volume.

From the contact point of view, a clear picture emerges when the aggregate is axially deformed. The initial state is isotropic in terms of contact vector orientations and contact loading. When the aggregate is sheared, within the range of deformation of our interest, the contact network is still approximately isotropic, while contact loadings show an alignment with the applied deformation along $\mathbf{e}_1$. Anisotropy in loading occurs and $\mathbf{e}_1$ becomes a preferential direction for the contact forces. Moreover, as seen in Fig. 1, the tangential component of the stress, q_T/p_0, reaches a plateau, e.g. [28, 33], which implies that, after about $\gamma/\Delta_0 \simeq 0.2$, the increment in tangential forces is zero, as we will show in the present contribution.

2.4 Incremental response

At four stages along the loading path, as indicated in Fig. 1, we calculate the incremental response of the aggregate.

In order to measure the components of the stiffness matrix A_{ijkm}, an infinitesimal strain $\delta\varepsilon_{km}$ is applied to the aggregate and the resulting change in stress is measured after sufficient relaxation [10]:

$$A_{ijkm} = \delta\sigma_{ij}/\delta\varepsilon_{km}. \tag{8}$$

3 Elastic and inelastic macroscopic behaviour

3.1 Axial-symmetric probes

We first focus on the incremental response with perturbations that maintain the symmetry generated by the axial symmetric loading. That is, $\delta\varepsilon_{22} = \delta\varepsilon_{33} = 0$, $\delta\varepsilon_{11} \neq 0$, so, adopting Voigt's notation,

$$A_{11} = \delta\sigma_{11}/\delta\varepsilon_{11} \tag{9}$$

and

$$A_{31} = \delta\sigma_{33}/\delta\varepsilon_{11}, \tag{10}$$

with $A_{31} = A_{21}$ for symmetry. We also distinguish between forward loading and unloading. In the former, $\delta\varepsilon_{11}$ is negative as it is in the axial-symmetric loading ($\varepsilon_{11} < 0$), while in the latter $\delta\varepsilon_{11}$ is positive ($\varepsilon_{11} > 0$).

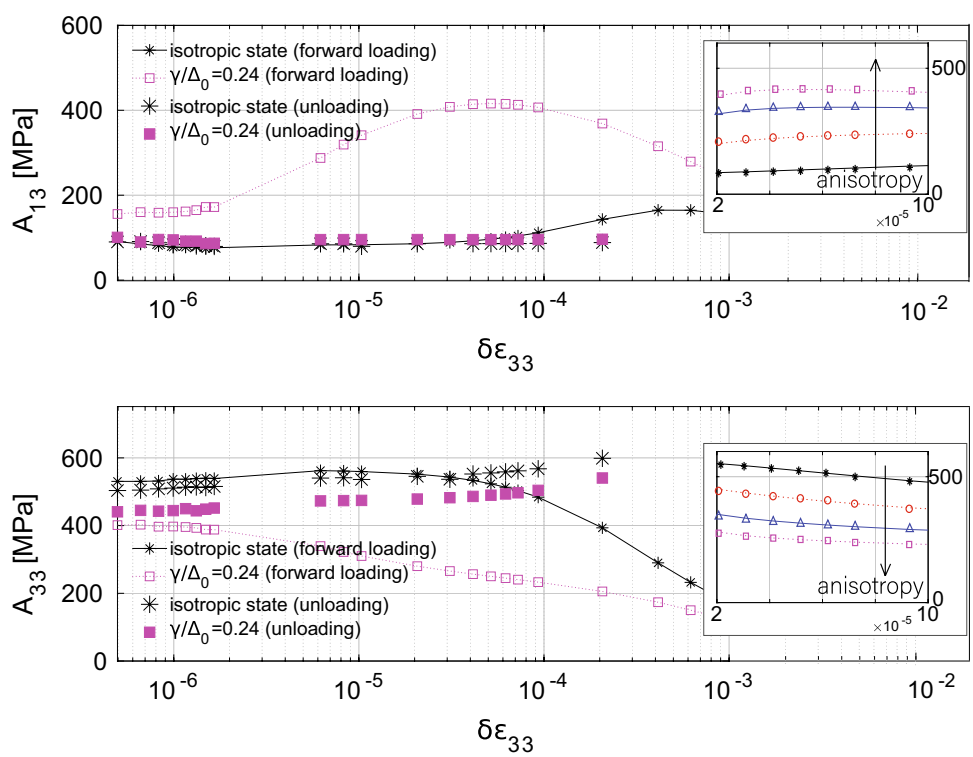

Fig. 5 Effective moduli A_{13} and A_{33} for different regimes of perturbation in two stressed states: isotropic and anisotropic state ($\gamma/\Delta_0 = 0.24$). In the insets the behaviour in the intermediate regime for all isotropic/anisotropic states, as indicated in Fig. 1 are shown

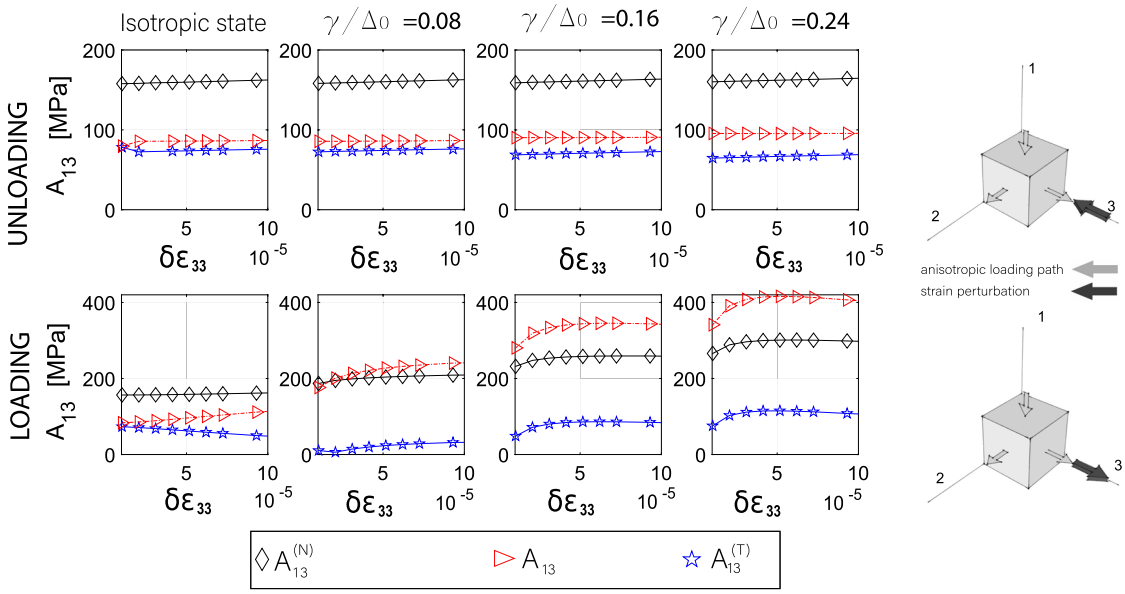

(a) A_{13} plotted in the second regime of perturbation: unloading and forward loading.

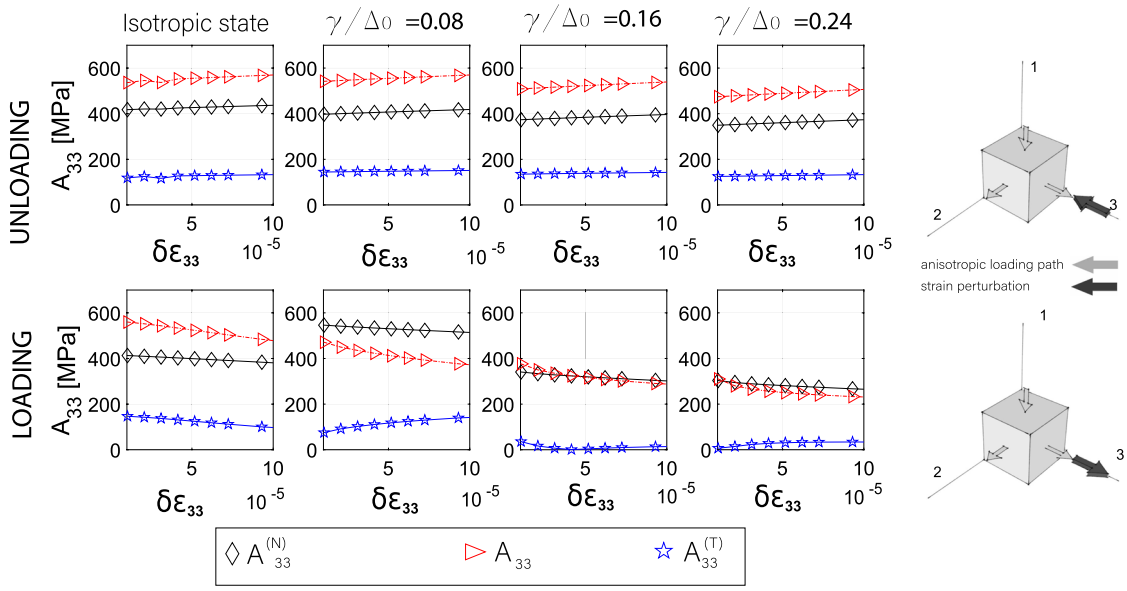

(b) A_{33} plotted in the second regime of perturbation: unloading and forward loading. In the forward loading, as anisotropy develops, the contribution of the tangential force in A_{33} becomes negligible.

Fig. 6 Effective moduli A_{13} and A_{33} versus strain amplitude

In Fig. 3 we plot the evolution with the strain of the moduli A_{31} and A_{11}, for the isotropic state and the anisotropic state associated with $\gamma/\Delta_0 = 0.24$.

In the first range of perturbation, $\delta\varepsilon_{11} \simeq 10^{-6}$, there is no difference between forward loading and unloading, irrespective of the state of the material, isotropic or anisotropic. That is, if the aggregate is incrementally strained with an extremely small perturbation all contacts behave elastically [16]. Instead, for slightly bigger probes, $\delta\varepsilon_{11} \simeq 10^{-5}$, we see a second plateau and a difference in the response between forward and unloading probes. While unloading probes seem weakly related with anisotropy, in the case of forward loading a pronounced dependency on the stress state appears, with A_{11} (A_{31}) decreasing (increasing) with anisotropy. Details of this second regime induced by forward loading are shown in the inset.It is noteworthy to mention that, during all the applied increments, we do not see any significant change in the coordination number as we will show in details later in the section Micromechanics.

An interesting feature appears in the second regime when we plot the moduli A_{11} and A_{31} partitioned in a normal and tangential part. $A_{11}^{(N)}$ and $A_{31}^{(N)}$ are the moduli inferred from the stress containing contributions from the normal component of the contact forces while $A_{11}^{(T)}$ and $A_{31}^{(T)}$ are related to the tangential component of the contact forces. In Fig. 4a, b we show details of the results: while in the unloading cases both moduli A_{11} and A_{31} have contributions from a normal and tangential part of the stress, the response to an incremental forward loading is mainly characterized by the normal contribution with a clear evidence for the anisotropic states in which q_T is constant (see Fig. 1). That is, the response is incrementally frictionless. At $\gamma/\Delta_0 \simeq 0.2$, where q_T/p_0 has reached its plateau, both $A_{11}^{(T)}$ and $A_{31}^{(T)}$ are almost zero. As the slope in q_N/p_0 changes with γ/Δ_0 so the moduli A_{11} and A_{31} vary. The transition between the two plateau, the first at very small deformation identified as the elastic regime and the second associated with the plastic regime, resembles what predicts by Rudnicki and Rice [9] in their yield-vertex constitutive model. That is, the transition represents a combination of an elastic response associated with contacts that still experience an elastic resistance and a plastic response characterized by zero incremental tangential resistance. The second plateau, also emphasized in Fig. 3, indicates instead that the response is plastic with no local, incremental tangential resistance. Something similar has been also pointed out by Tamagnini et al. [37], in a continuum model, through a bounding surface to be distinguished from the classical yield surface.

3.2 Probes with no symmetry

We now look at the incremental response of the aggregate when forward loading and unloading probes are applied along $\mathbf{e}_3$, $\delta\varepsilon_{33} \neq 0$ with $\delta\varepsilon_{11} = \delta\varepsilon_{22} = 0$. We can determine:

$$A_{13} = \delta\sigma_{11}/\delta\varepsilon_{33} \tag{11}$$

and

$$A_{33} = \delta\sigma_{33}/\delta\varepsilon_{33}. \tag{12}$$

Because of the symmetry associated with the axial loading along $\mathbf{e}_1$, probes along $\mathbf{e}_2$ and $\mathbf{e}_3$ produces the same response, so

$$A_{13} = A_{12} \tag{13}$$

and

$$A_{33} = A_{22}. \tag{14}$$

In Fig. 5 we plot the results for A_{13} and A_{33}. Again we note a first elastic regime, at $\delta\varepsilon_{33} \simeq 10^{-6}$, in which there is no difference between incremental loading and unloading.

We recall that the axial-loading (see Fig. 1) is carried out by applying a strain $\varepsilon_{11} < 0$, with $\varepsilon_{22} = \varepsilon_{33} > 0$ to maintain a constant confining pressure; so unloading probe now means $\delta\varepsilon_{33} < 0$ while forward incremental loading means $\delta\varepsilon_{33} > 0$. These incremental conditions do not reproduce the symmetry induced by the uniaxial loading. In the Fig. 4b we note again a second plateau associated with the *inelastic* regime for A_{13}. When we look closely at A_{33}, we observe a clear elastic regime, followed by a rather narrow second plateau. In the insets, we show the dependence of the forward loading probing on anisotropy.

Furthermore, we look at the normal and tangential contributions of A_{13} and A_{33} versus strain. In Fig. 4a, b, we observe that the behavior of the partitioned moduli differs

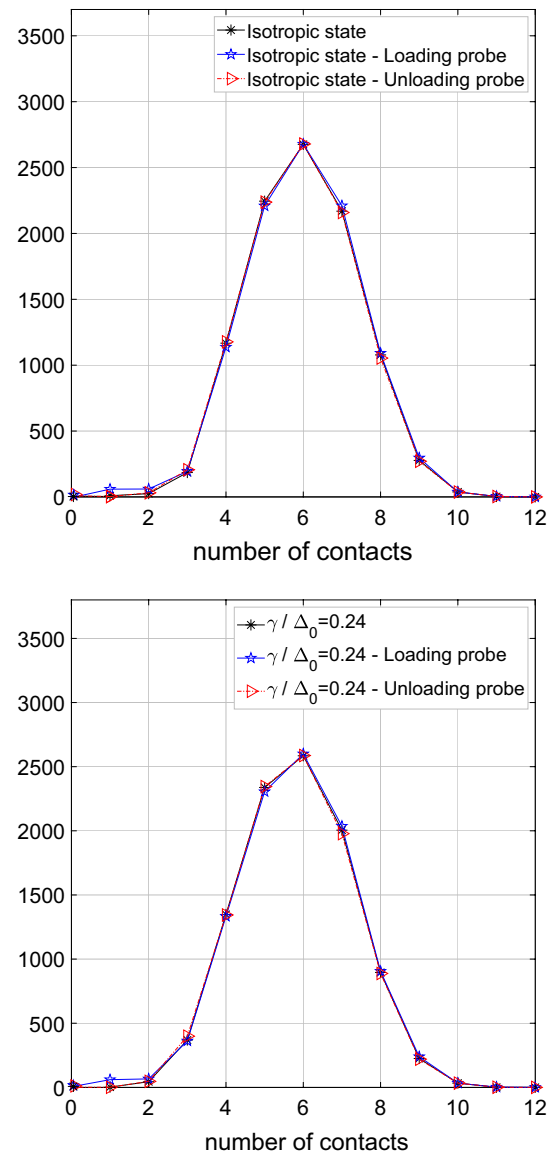

Fig. 7 Contact distribution functions for (top) isotropic, $k_0 = 5.95$, and (bottom) anisotropic, $k = 5.78$, with $\gamma/\Delta_0 = 0.24$. For both cases, the contact distributions of the initial packing, after incremental forward loading and unloading are reported

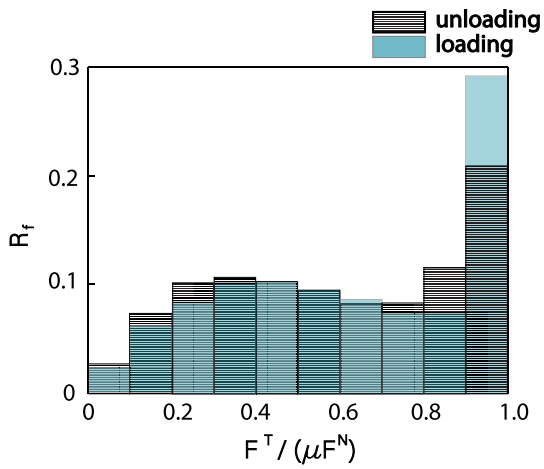

Fig. 8 Relative frequency of mobilized friction during incremental forward loading and unloading, for the configuration at $\gamma/\Delta_0 = 0.24$

between A_{11} and A_{31}. The contribution associated with the tangential part of the contact force does not vanish because we are not deforming particles along the same path of the axial-symmetric loading. That is, some contacts that were sliding under the axial loading are now behaving elastically because the probe does not maintain the same symmetry.

Finally, Fig. 6b shows that the tangential contribution of A_{33} in the *inelastic* regime is again negligible, suggesting an incrementally frictionless behavior.

In all cases examined, increments larger than 10^{-4} produces a non-linear regime, more evident in case of anisotropy, in which the response depends on the amplitude of incremental strain ([19, 36, 37]). Moreover, in the regime of deformation where the *inelastic* stiffness is defined, when anisotropy develops, the aggregate exhibits the loss of the major symmetry in the macroscopic stiffness, $A_{13} \neq A_{31}$. This is a crucial condition to determine localization in a granular material [9, 38, 39].

Our results are in line with previous findings in [15, 17] and [22]. Specifically, the authors in [15] have shown that only isotropic samples conform to the hypotheses beyond elasto-plastic constitutive models, while major deviations are observed as soon as anisotropic stress history is considered. Figs. 3, 4, 5 in the present work (a simpler context in which probes are along two directions only) provide a similar message, with the presence of an intermediate regime neither totally elastic or plastic in case of anisotropic samples. In such *inelastic* regime, stress and strain increments may loose alignement under uniaxial probes along y_1 and y_3, imposed over the initial triaxial stress state. In [17] DEM simulations show the outmost importance of the rotation with respect to the axis of pre-loading on the incremental response of a granular material, in terms of the definition of a flow direction and non-associated character of the flow rule, i.e. loss of major symmetry as in our paper. However, we found the loss of major symmetry already happens in what we call an "*inelastic* regime", even before the friction is largely mobilized in the plastic regime. Finally, in their extensive and accurate work, Kuhn et al. [22] show that five over six principles of conventional elasto-plasticity fail when tested against preloaded anisotropic granular materials. The lost principles include direction and magnitude of the strain increments, the yield criterion as well as the separation of strain increments into elastic and plastic. Our findings in the *inelastic* regime conform to the analysis in [22], while it still supports the idea of a fully elastic regime for very small strain increments. All these works suggest the need of more complex constitutive models for a comprehensive description of granular materials (e.g. multi-mechanism plasticity or tangential plasticity).

4 Micromechanics

4.1 Micromechanical characterization of elastic and inelastic regimes

In order to characterize the difference between the material response during probing in the *inelastic* regime, we investigate the micro-structure of the aggregate, with special focus on the number of contacts, mobilised friction at the contacts.

In Fig. 7 we compare the contact distribution functions of the initial relaxed configuration with those after incremental *inelastic* forward loading and unloading, in the isotropic and anisotropic ($\gamma/\Delta_0 = 0.24$) packings. As an example we show here the response under axial-symmetric probe, $\delta\varepsilon_{11}$, as in Sect. 3.1. Interestingly, we find that the contact distribution collapses on the initial configuration, irrespective of the probing direction. That is, the contact network is not affected by either unloading or forward *inelastic* probes. This implies that the coordination number, i.e. the mean of the functions, as well as the fluctuation in the number of contacts coincide between the packings. Moreover, when comparing the two figures, the influence of anisotropy appears to be negligible.

Furthermore, in Fig. 8, we look at the mobilized friction during incremental forward loading and unloading. We define the relative frequency R_f as the number of contacts with a given ratio between tangential and normal forces, $F^T/\mu F^N$, normalized by the total number of contacts, where $F^T/\mu F^N = 1$ means sliding. The figure highlights that, despite the contact network stays unchanged under probing (see Fig. 7), slippage occurs within the contact area and contacts reach the onset of sliding. An higher percentage of contacts, about 30%, sit in proximity of sliding, in the case of incremental *inelastic* forward loading.

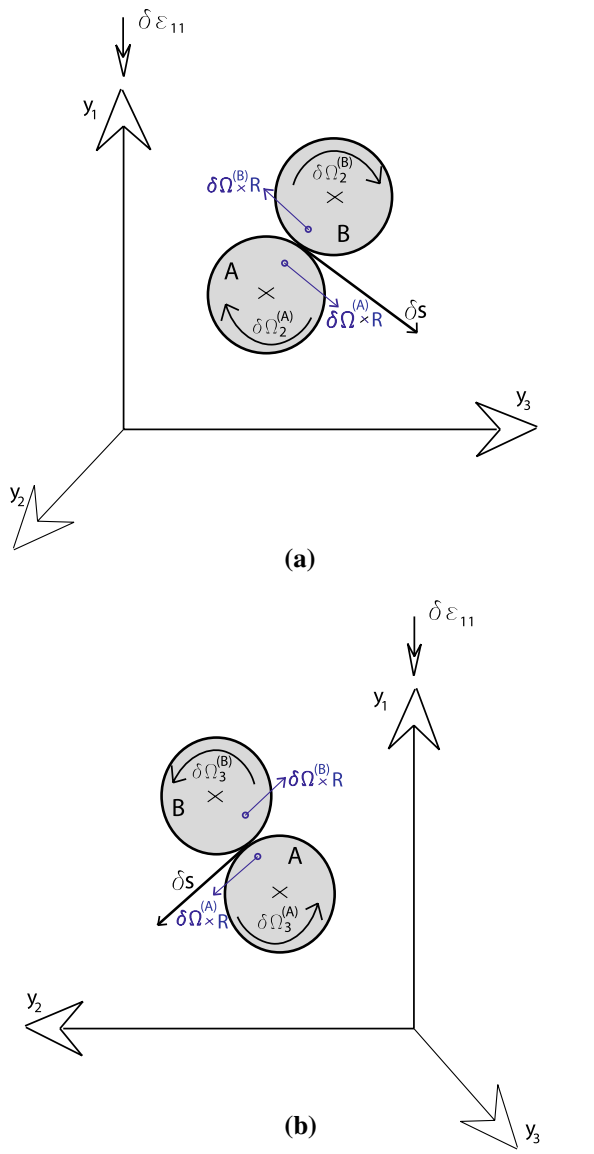

Fig. 9 The kinematics of a typical pair in which, given the proper sign of the rotations and δs, it is possible to realize a relative, tangential, contact displacement equal to zero: **a** projection on the plane $y_1 - y_3$; **b** projection on the plane $y_1 - y_2$.

4.2 Incremental sliding and rotations

As forward step, we study the kinematics at the microscale, in terms of contact sliding and particle rotations. We focus on the axial-symmetric probes as in Sect. 3.1, and propose a micromechanical interpretation to explain why the tangential part of the moduli becomes zero under incremental forward loading, see Fig. 4a, b. We show that the tangential contribution of A_{11} and A_{31} disappears because particles slide and/or roll so the incremental tangential displacement become

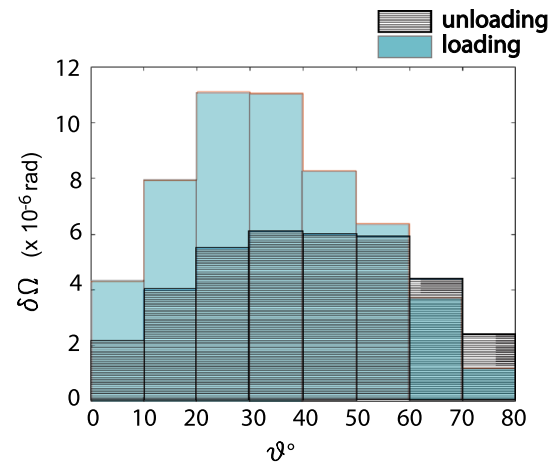

Fig. 10 Average rotations $\delta\Omega = \delta\Omega_3 = -\delta\Omega_2$ evaluated in each strip $\Delta\theta$ in the first octant, $0 \le \phi \le \pi/2$, in cases of forward incremental loading and unloading

zero. The analysis is motivated by a theoretical framework able to describe the elasticity of granular materials based upon micromechanics and the role of fluctuations, as given in [21].

Let us examine in details the incremental forward loading at $\gamma/\Delta_0 = 0.24$. Following [21], we can express the incremental relative contact displacement between a typical pair A and B as

$$\delta u_i^{(BA)} = \delta c_i^{(B)} - \delta c_i^{(A)} - \frac{1}{2}\varepsilon_{iqk}\left(\delta\omega_q^{(A)} + \delta\omega_q^{(B)}\right)d_k^{(BA)} \tag{15}$$

where δc_i and $\delta\omega_i$ are, respectively, the increment in translation and the increment in rotation of the particle. The tangential component of the contact force is

$$\delta F_i^T = K_T^{(BA)}\left(\delta u_i^{(BA)} - \delta u_q^{(BA)}\hat{d}_q^{(BA)}\hat{d}_i^{(BA)}\right) \tag{16}$$

in which K_T is the tangential contact stiffness

$$K_T^{(BA)} = \frac{2G(2R)^{1/2}}{2-\nu}\rho^{(BA)1/2} \tag{17}$$

and $\rho^{(BA)} = \delta u_i^{(BA)}\hat{d}_i^{(BA)}$ is the overlap between contacting particles. With Eq. (15), the incremental tangential component of the contact force becomes

$$\delta F_i^T = K_T^{(BA)}\left[\delta s_i^{(BA)} - \frac{1}{2}\epsilon_{iqk}\left(\delta\omega_q^{(A)} + \delta\omega_q^{(B)}\right)d_k^{(BA)}\right] \tag{18}$$

in which $\delta s_i^{(BA)}$ is the incremental tangential displacement associated with the translation of the centers. Because of equilibrium, La Ragione and Jenkins [24] show that fluctuations in spin rather than in translation play a major role. Consequently, we express $\delta s_i^{(BA)}$ in terms of the incremental

Table 1 Incremental forward loading: in each strip, centered at different angle θ, we measure the average tangential displacement $< \delta s_1 >_\theta$ (first row) and the average rotations so their difference is a_L (second row). Both terms, $< \delta s_1 >_\theta$ and a_L are normalized by 2R

	$\theta = 5^o$	$\theta = 15^o$	$\theta = 25^o$	$\theta = 35^o$	$\theta = 45^o$	$\theta = 55^o$	$\theta = 65^o$	$\theta = 75^o$
$< \delta s_1 >_\theta \times 10^5$	−0.03	−0.26	−0.65	−1.08	−1.41	−1.54	−1.39	−0.97
$a_L \times 10^5$	−0.01	−0.005	−0.05	−0.27	−0.69	−0.88	−0.93	−0.84

Table 2 Incremental unloading: as in Table 1 but with a_U instead of a_L

	$\theta = 5^o$	$\theta = 15^o$	$\theta = 25^o$	$\theta = 35^o$	$\theta = 45^o$	$\theta = 55^o$	$\theta = 65^o$	$\theta = 75^o$
$< \delta s_1 >_\theta \times 10^5$	0.03	0.26	0.65	1.08	1.41	1.54	1.39	0.97
$a_U \times 10^5$	0.008	0.12	0.36	0.64	0.87	0.91	0.89	0.69

average strain, $\delta\varepsilon_{ij}$, while the rotations include only fluctuations because the average is zero [40]:

$$\delta s_i^{(BA)} = \delta\varepsilon_{ij} d_j^{(BA)} - \delta\varepsilon_{ql} d_q^{(BA)} \hat{d}_l^{(BA)} \hat{d}_i^{(BA)}. \tag{19}$$

When the incremental tangential displacement associated with the translation of the centers is equal to the corresponding contribution associated with particle rotations rolling occurs; that is:

$$\delta s_i^{(BA)} = 1/2\epsilon_{iqk}\left(\delta\omega_q^{(A)} + \delta\omega_q^{(B)}\right) d_k^{(BA)}. \tag{20}$$

Therefore, the condition for zero incremental tangential force,δF^T , occurs with rolling, Eq. (20), or sliding, $F^T = \mu F^N$.

We want to test our findings by comparing the amount of rolling and sliding particles during incremental axial-symmetric forward loading and unloading. We recall that y_1 is the axis of anisotropy with the unit contact vector defined in terms of the polar angle, θ, and ϕ so $\hat{d} = (\cos\theta, \sin\theta\cos\phi, \sin\theta\sin\phi)$. As said earlier, $\delta\omega$ represents a fluctuation being the average rotation over all particles zero. We measure these fluctuations by making a partition in θ for all ϕ. In Fig. 9 we sketch, with the proper signs, the interaction of a typical pair.

We take M_p pairs of contacting particles whose contact vectors, $\hat{d}_i$, are within a strip of width $\Delta\theta$ and $0 \le \phi \le \pi/2$. With incremental forward loading $\delta\varepsilon_{11} < 0$ or unloading $\delta\varepsilon_{11} > 0$ applied, we measure, for all pairs, the rotations and the corresponding average in the strip, $\delta\Omega$. That is,

$$\delta\Omega_i = \frac{1}{2M_p} \sum_{\hat{d}^{(BA)} \subset [\Delta\theta; 0 \le \phi \le \pi/2]}^{M_p} (\delta\omega_i^A + \delta\omega_i^B). \tag{21}$$

We obtain $\delta\Omega_1$ approximately zero while $\delta\Omega_2 = -\delta\Omega_3$. The numerical results, with $\delta\varepsilon_{11} = \pm 4 \times 10^{-5}$, i.e. in the *inelastic* regime, for both forward loading and unloading are shown in Fig. 10. The figure shows clear differences in the microscale kinematic between the two cases. While the average fluctuation $\delta\Omega_2$ is comparable for high θ, it becomes higher for forward loading than unloading when $\theta < 50°$.

The results can be extended, by symmetry, to the other octants, $\phi > \pi/2$. We take the average of the incremental tangential displacement in each band, so Eq. (19) can be written

$$< \delta s_1 >_{\theta; 0 \le \phi \le \pi/2} = \delta\varepsilon_{11} \cos\theta - \delta\varepsilon_{11} \cos^3\theta \tag{22}$$

for $\theta = 5^o, 15^o, 25^o, \ldots 75^o$, while for the rotation contribution, $S_i = 1/2\epsilon_{iqk}\left(\delta\omega_q^{(A)} + \delta\omega_q^{(B)}\right) d_k^{(BA)}$, we define the average over the strip centered in θ

$$< S_1 >_{\theta; 0 \le \phi \le \pi/2} = \frac{2}{\pi}\left(\Omega_2 - \Omega_3\right) \sin\theta \tag{23}$$

where we have employed the average over ϕ

$$\frac{2}{\pi}\int_0^{\pi/2} \sin\phi d\phi = \frac{2}{\pi}\int_0^{\pi/2} \cos\phi d\phi = \frac{2}{\pi}. \tag{24}$$

We could have considered an average that accounts for the fraction of contacts in each strip but the results will not differ significantly.

The difference of the averages in each strip is

$$a = < \delta s_1 >_{\theta; 0 \le \phi \le \pi/2} - < S_1 >_{\theta; 0 \le \phi \le \pi/2}. \tag{25}$$

The corresponding numerical results, for forward probing $\delta\varepsilon_{11} = 4 \times 10^{-5}$, are reported in Table 1. In the strips between $0 \le \theta \le 30^o$ the difference in the average, a_L, is approximately zero which implies that in that range contacts experience rolling rather than sliding. For $30^o \le \theta \le 80^o$ particles mostly slide. In Table 2 we report the same parameters as in Table 1 but in case of unloading. Here the parameter a_U is always different from zero, implying that a contribution associated with F^T is always present. This is confirmed by A_{11}^T and A_{31}^T different from zero in Fig. 4a, b.

The results in Table 1 are shown in a different fashion in Fig. 11, where we plot, the relative frequency R_f of sliding contacts in each strip, i.e., the number of contacts in the

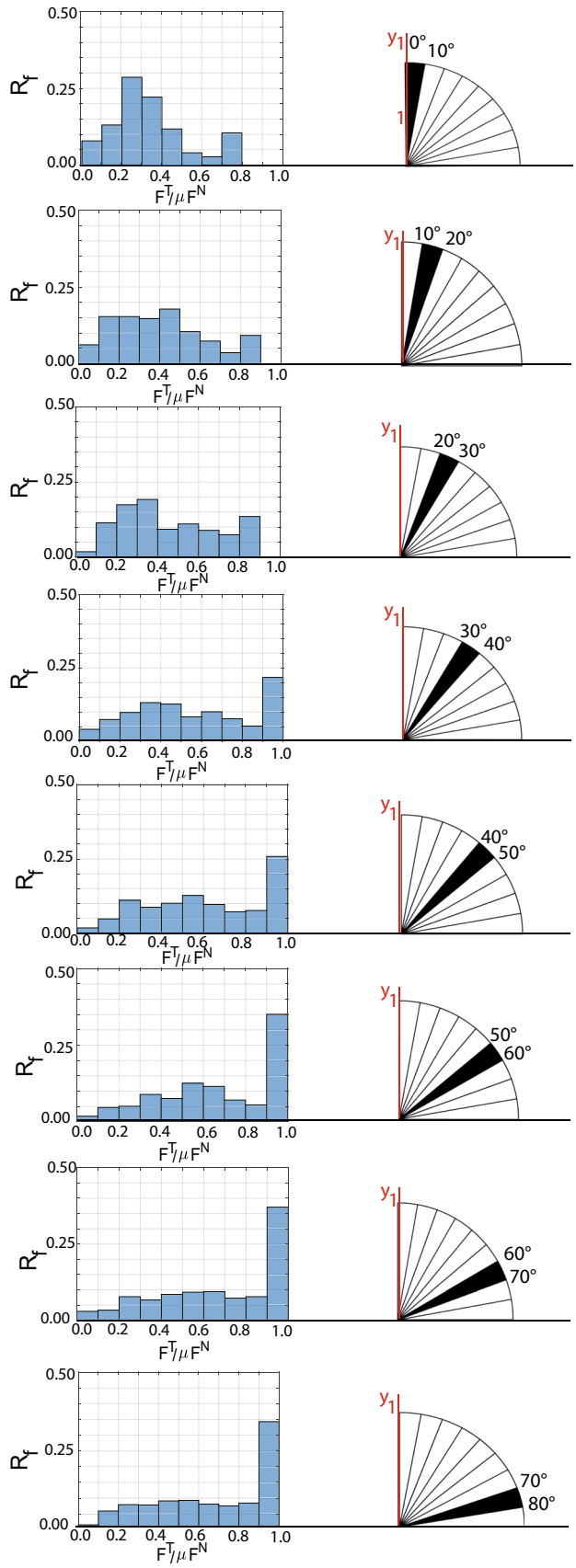

Fig. 11 Relative frequency R_f associated with the normalized sliding ▸ contacts in each strip in case of incremental forward loading

sliding condition normalized by the number of contact in that strip. For $0 \leq \theta \leq 30^o$ sliding does not occur while for $\theta \geq 30^o$ becomes important. Data in the strip $80^o \leq \theta \leq 90^o$ have not been included here as the number of contacts is negligible.

5 Conclusions

We have analyzed the behavior of a sheared granular material via DEM numerical simulations. Anisotropy is developed in the sheared granular assembly, in a regime of deformation in which the contact network does not change. In particular, we have focused on the incremental response of the aggregate when probes, different in both direction and amplitude, are applied along the shear path.

The material behaviour depends on the smallness of the applied probes in a non-trivial way. If the amplitude of the probe is extremely small then A_{ijkm} is essentially an elastic tensor, irrespective of forward or unloading conditions. If the probes are bigger, then a difference between unloading and forward probes occurs. Consequently the response of the aggregate, when incrementally forward strains are applied, transits from "perfectly" elastic to non-linear strain regime, through an intermediate *inelastic* state in which the macroscopic stiffness components, independent of strain amplitudes, are different from the elastic moduli obtained via unloading probing. Through a micro-mechanics analysis we show that the overall incremental response of the anisotropic aggregate, under particular incremental perturbations, is independent of the tangential forces between particles and mechanisms like rolling or slide occur.

Funding Open access funding provided by Politecnico di Bari within the CRUI-CARE Agreement.

Compliance with ethical standards

Conflict of interest The authors declare that They have no conflict of interest.

Open Access This article is licensed under a Creative Commons Attribution 4.0 International License, which permits use, sharing, adaptation, distribution and reproduction in any medium or format, as long as you give appropriate credit to the original author(s) and the source, provide a link to the Creative Commons licence, and indicate if changes were made. The images or other third party material in this article are included in the article's Creative Commons licence, unless indicated otherwise in a credit line to the material. If material is not included in the article's Creative Commons licence and your intended use is not permitted by statutory regulation or exceeds the permitted use, you will need to obtain permission directly from the copyright holder. To view a copy of this licence, visit http://creativecommons.org/licenses/by/4.0/.

References

1. Behringer, R.P., Jenkins, J.T.: (Editors), Powders and Grains (Balkema, Rotterdam) 1997; Jaeger H. M.and Nagel S. R., Science, 255, 1523 (1992)
2. Guyer, R.A., Johnson, P.A.: Physics Today **52**, 30 (1999)
3. Cundall, P.A., Strack, O.D.L.: A discrete numerical model for granular assemblies. Geotechnique **29**, 47–65 (1979)
4. O'Donovan, J., Ibraim, E., O'Sullivan, C., Hamlin, S., Wood, D.M., Marketos, G.: Micromechanics of seismic wave propagation in granular materials. Granul. Matter **18**(3), 56 (2016)
5. Marketos, G., O'Sullivan, C.: A micromechanics-based analytical method for wave propagation through a granular material. Soil Dyn. Earthq. Eng. **45**, 25–34 (2013)
6. Burland, J.B.: Small is beautiful: the stifness of soils at small strains. Can. Geotech. J. **26**, 499–516 (1989)
7. Einav, I., Puzrin, A.M.: Pressure dependent elasticity and energy conservation in elastoplastic models for soils. Geotech. Geoenviron. Eng. **130**, 81–92 (2004)
8. Houlsby, G.T., Amorosi, A., Rojas, E.: Elastic moduli of soils dependent on pressure: a hyperelastic formulation. Géotechnique **55**, 383–392 (2005)
9. Rudnicki, J., Rice, J.R.: Conditions for the localization of deformations in pressure sensitive dilatant materials. J. Mech. Phys. Solids **23**, 371–394 (1975)
10. Magnanimo, V., La Ragione, L., Jenkins, J.T., Wang, P., Makse, H.A.: Characterizing the shear and bulk moduli of an idealized granular material. Europhys. Lett. **81**, 34006–27 (2008)
11. Makse, H.A., Gland, N., Johnson, D.L., Schwartz, L.: Why Effective Medium Theory Fails in Granular Materials. Phys. Rev. Lett. **83**, 5070 (1999)
12. Makse, H.A., Gland, N., Johnson, D.L., Schwartz, L.: Granular packings: Nonlinear elasticity, sound propagation, and collective relaxation dynamics. Phys. Rev. E **70**, 061302 (2004)
13. Alonso-Marroquin, F., Luding, S., Herrmann, H.J., Vardoulakis, I.: Role of anisotropy in the elastoplastic response of a polygonal packing. Phys. Rev. E **71**, 051304 (2005)
14. Thornton, C., Zhang, L.: On the evolution of stress and microstructure during general 3D deviatoric straining of granular media. Géotechnique **60**(5), 333–341 (2010)
15. Calvetti, F., Viggiani, G., Tamagnini, C.: A numerical investigation of the incremental behavior of granular soils. Riv. Italiana Geotec. **3**, 11–29 (2003)
16. Agnolin, I., Roux, J.N.: Internal states of model isotropic granular packings. III. Elastic properties. Phys. Rev. E **76**, 061304 (2007)
17. Froiio, F., Roux, J.N.: Incremental response of a model granular material by stress probing with DEM simulations AIP Conference Proceedings **1227**(1), 183–197 (2010)
18. Mouraille, O., Mulder, W.A., Luding, S.: Sound wave acceleration in granular materials. J. Stat. Mech. Theory Exp. **2006**(07), P07023–P07023 (2006)
19. Cheng, H., Luding, S., Saitoh, K., Magnanimo, V.: Elastic wave propagation in dry granular media: effects of probing characteristics and stress history. Int. J. Solid Struct. (2019). https://doi.org/10.1016/j.ijsolstr.2019.03.030
20. La Ragione, L., Oger, L., Recchia, G., Sollazzo, A.: Anisotropy and lack of symmetry for a random aggregate of frictionless, elastic particles: theory and numerical simulations. Proc. R. Soc. A Math. Phys. Eng. Sci. **471**, 13 (2015)
21. La Ragione, L.: The incremental response of a stressed, anisotropic granular material: loading and unloading. J. Mech. Phys. Solids **95**, 147–168 (2016)
22. Kuhn, M.R., Daouadji, A.: Multi-directional behavior of granular materials and its relation to incremental elasto-plasticity. Int. J. Solids Struct. **152–153**, 305–323 (2018)
23. Luding, S.: Molecular dynamics simulations of granular materials. In: Hinrichsen, H., Wolf, D.E. (eds.) Phys. Granul. Media, pp. 299–324. Wiley VCH, Weinheim, Germany (2004)
24. La Ragione, L., Jenkins, J.T.: The initial response of an idealized granular material. Proc. R. Soc. A Math. Phys. Eng. Sci. **473**(2079), 735–758 (2006)
25. Jenkins, J.T., Johnson, D., La Ragione, L., Makse, H.: Fluctuations and the effective moduli of an isotropic, random aggregate of identical, frictionless spheres. J. Mech. Phys. Solids **53**, 197–225 (2005)
26. La Ragione, L., Magnanimo, V.: Evolution of the effective moduli of an anisotropic, dense, granular material. Granul. Matter **14**, 749–757 (2012)
27. Cundall, P.A.: Computer simulations of dense sphere assemblies. In: Satake, M., Jenkins, J.T. (eds.) Micromechanics of Granular Materials, pp. 113–125. Elsevier, Amsterdam (1988)
28. Thornton, C., Anthony, S.J.: Quasi-static deformation of particulate media. Philos. Trans. R. Soc. Lond. Ser. A **356**(1747), 2763–2782 (1998)
29. Khalili, M.H., Roux, J.N., Pereira, J.M., Brisard, S. and Bornert M.: Numerical study of one-dimensional compression of granular materials. II. Elastic moduli, stresses, and microstructure, Physical Review E, 95, 032908 (2017)
30. Mindlin, R.D.: Compliance of elastic bodies in contact. J. Appl. Mech. **16**, 259–268 (1949)
31. Thornton, C., Randall, C.W.: Applications of Theoretical Contact Mechanics to Solid Particle System Simulation, in Micromechanics of Granualr Materials, Proceedings of the U.S./Japan Seminar on the Micromechanics of Granular Materials, Sendai-Zao, Japan, October 26-30, 1987, Edited by Masao Satake, James T. Jenkins, 20, pp. 133-142 (1988)
32. Love, A.E.H.: A treatise on the mathematical theory of elasticity. Cambridge University Press, Cambridge (1927)
33. Jenkins, J.T., Strack, O.D.L.: Mean-field inelastic behavior of random arrays of identical spheres. Mech. Mater. **16**, 25–33 (1993)
34. Torquato, S.: Random Heterogeneous Materials, 1. Springer-Verlag, NewYork (2001)
35. Jenkins, J.T., Cundall, P.A., Ishibashi, I.: Micromechanical modeling of granular materials with the assistance of experiments and numerical simulations. In: Biarez, J., Gourves, R. (eds.) Powders and Grains, pp. 257–264. Balkema, Rotterdam (1989)

36. Santamarina, J.C., Cascante, G.: Stress anisotropy and wave propagation: a micromechanical view. Can. Geotech. J. **33**(5), 770–782 (1996)
37. Tamagnini, C., Calvetti, F., Viggiani, G.: An assessment of plasticity theories for modeling the incrementally nonlinear behavior of granular soils. J. Eng. Math. **52**(1), 265–291 (2005)
38. La Ragione, L., Prantil, V.C., Jenkins, J.T.: A micromechanical prediction of localization in a granular material. J. Mech. Phys. Solids **83**, 146–159 (2015)
39. Nicot, F., Daouadji, A., Laouafa, F., Darve, F.: Second-order work, kinetic energy and diffuse failure in granular materials. Granul. Matter **13**(1), 19–28 (2011)
40. La Ragione, L., Jenkins, J.T.: The influence of particle fluctuations on the average rotation in an idealized granular material. J. Mech. Phys. Solids **57**, 1449–1458 (2009)

Publisher's Note Springer Nature remains neutral with regard to jurisdictional claims in published maps and institutional affiliations.